Environmental Science & Technology

Article

pubs.acs.org/est

Dissolution and Carbonation of Portlandite [$Ca(OH)_2$] Single Crystals

Encarnación Ruiz-Agudo,*[,†,‡] Krzysztof Kudłacz,[§,†] Christine V. Putnis,[‡] Andrew Putnis,[‡] and Carlos Rodriguez-Navarro[†]

[†]Department of Mineralogy and Petrology, University of Granada, Fuentenueva s/n, 18071 Granada, Spain

[‡]Institut für Mineralogie, WWU Münster, Corrensstrasse 24, 48147 Münster, Germany

[§]Institute of Metallurgy and Materials Science, Polish Academy of Sciences, Reymonta 25, 30-059 Kraków, Poland

Supporting Information

ABSTRACT: The dissolution and carbonation of portlandite ($Ca(OH)_2$) single crystals was studied by a combination of in situ Atomic Force Microscopy, Scanning Electron Microscopy, and two-dimensional X-ray diffraction. The dissolution of portlandite {0001} surfaces in water proceeds by the formation and expansion of pseudohexagonal etch pits, with edges parallel to ⟨100⟩ directions. Etch pits on {010} surfaces are elongated along ⟨001⟩, with edges parallel to ⟨101⟩. The interaction between carbonate-bearing solutions and portlandite results in the dissolution of the substrate coupled with the precipitation of thick islands of $CaCO_3$ that appear oriented on the portlandite substrate. Ex situ carbonation of portlandite in contact with air results in the formation of pseudomorphs that fully preserve the external shape of the original portlandite single crystals. Our observations suggest that portlandite carbonation in contact with air and carbonate-bearing solutions occurs by a similar mechanism, i.e. coupled dissolution−precipitation. Calcite grows epitaxially on {0001} portlandite surfaces with the following orientation: $\langle 001\rangle_{Cc} \| \langle 001\rangle_{Port}$. Apparently, no porosity is generated during the reaction, which progresses through the formation of fractures. Our results are of relevance to many processes in which the carbonation of portlandite takes place, such as CO_2 capture and storage or the carbonation of cementitious materials.

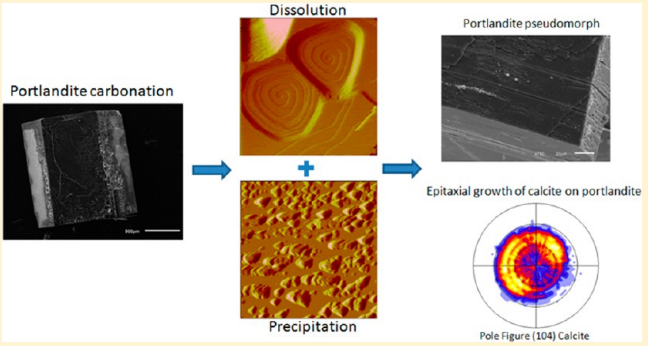

INTRODUCTION

Portlandite has a CdI_2-type structure (trigonal, space group $P\bar{3}m1$), and it is one of the simplest hydrous minerals along with isostructural brucite ($Mg(OH)_2$), whose dissolution and carbonation have been recently studied.[1−3] The layered structure of these hydroxides is very similar to that of clay minerals, which are among the most abundant components of the Earth's outer crust.[4] Unlike clay minerals and brucite, the occurrence of portlandite is, however, minimal in natural earth surface environments as it rapidly carbonates in contact with atmospheric CO_2 to give calcium carbonate. Nevertheless, understanding the dissolution behavior of portlandite is relevant to obtain insights into the dissolution processes of other layered minerals with environmental significance such as serpentine (used for CO_2 sequestration)[5] or hydrotalcite-like phases (used for the capture of toxic metals).[6] Similarly, a better understanding of the carbonation of such a hydroxide is relevant to a range of industrial and technical processes spanning from the setting and degradation of cementitious materials[7] to ex situ CO_2 capture and storage (CCS) by mineralization of carbonates.[8]

In particular, the study of portlandite reactivity (dissolution and carbonation) is crucial for understanding the behavior of artificial mineral assemblages such as mortars or cements. Carbonation of portlandite is the key process in the setting of traditional lime mortars used for building purposes since the advent of pyrotechnology ca. 12000 years ago.[9] Textural and microstructural characteristics of the newly precipitated calcium carbonate and its evolution during carbonation determine the physical and mechanical properties of lime mortars,[10] which are currently the choice as compatible materials for remediation in the conservation of the built heritage.[11] The carbonation of portlandite is also critical during the setting of plain concrete, since the calcite formed is less soluble than the portlandite which it replaces.

During the reaction of cement with water, the fresh paste becomes supersaturated with respect to portlandite which precipitates in the bulk of the hardened cement paste as well as a thin crystalline layer on aggregate and reinforcement steel surfaces. This interfacial portlandite plays a critical role in the mechanical resistance of reinforced concrete, and it also protects it from corrosion.[12] Degradation of concrete by "leaching" is usually associated with the infiltration of low-pH

Received: May 10, 2013
Revised: August 4, 2013
Accepted: August 5, 2013
Published: August 5, 2013

aqueous solutions, promoting the dissolution of hydrates.[13] This process leads to an important increase in cement porosity,[14] which may result in the deterioration of its elastic properties and the material strength. Furthermore, the access of these "corrosive" solutions will be facilitated by the increased porosity, further favoring degradation by a positive feedback loop. Degradation by dissolution of cement components such as portlandite, which typically accounts for ca. 15−20 wt % of set cement,[7] is a particularly important problem in concrete structures which are in contact with aqueous solutions during long periods of time, such as dams or radioactive waste disposal facilities.[13] Dissolution of portlandite also affects the long-term behavior of Portland cement. Cement is known to react strongly with CO_2-rich fluids, changing its mineralogy. This makes cement wells potential weak points in the geological sequestration of CO_2.[7] The carbonation of portlandite is a key reaction during ex situ CCS by mineralization of alkaline Ca-rich industrial wastes such as oil-shale ash,[15] cement kiln dust,[16] fly ash,[17] steel slag,[18] and paper sludge incineration ash.[8]

Knowledge regarding the mechanisms of portlandite dissolution and carbonation is critical for the evaluation of the long-term behavior of lime mortars and cement materials as well as for the design of remediation protocols. It is also critical to evaluate the potential and optimization of CCS using industrial alkaline wastes.

Despite the wide range of implications of portlandite reactivity, studies on portlandite carbonation from a mechanistic point of view are strikingly scarce, however. It is well-known that saturated solutions of calcium hydroxide readily carbonate in the presence of CO_2, and this aqueous phase route for carbonation has been exploited for the precipitation of calcium carbonate.[10] However, the limited solubility of portlandite (K_{sp} = 5.02 × 10^{-6}, at 25 °C and 1 atm) implies that during carbonation of $Ca(OH)_2$-rich systems such as cement, lime mortars, or industrial wastes, only a small fraction of $Ca(OH)_2$ will be in solution. Thus, carbonation would mostly involve the direct reaction with portlandite crystals. Remarkably, there is an ongoing controversy regarding the mechanisms of portlandite crystals carbonation. While Moorehead[19] suggests that carbonation of $Ca(OH)_2$ pastes in a CO_2 atmosphere (pCO_2 1 atm, 25 °C) is a solid-state reaction, Johnston and Glasser[20] suggest that it occurs via dissolution/precipitation rather than by a solid-state reaction. This latter contention is consistent with several studies showing that carbonation of $Ca(OH)_2$ crystals at room T requires the presence of H_2O.[12,21] Related to this, there is a significant lack of knowledge regarding the possible crystallographic control on the advancement of the carbonation reaction (i.e., epitaxy vs topotaxy). Gillott[22] suggested that the carbonation of portlandite crystals may be a topotactic transition, in agreement with Stepkowska[23] who suggests that carbonation in air occurs via a solid-state substitution of OH^- by CO_3^{2-}, this resulting in a change of d_{001} spacing of the portlandite structure. Montes-Hernandez and co-workers[24] also report a solid-state reaction for nanosized portlandite crystals transforming into nanosized calcite. However, the experimental techniques used in these works preclude the possibility of determining the exact crystallographic relationship between parent and product phases and thus are not able to establish unambiguously the mechanism of portlandite carbonation. The observations reported could be the result of both a solid-state reaction, which would imply a topotactic relationship between reactant and product phases, or a coupled dissolution−precipitation reaction, which would be related to an epitaxial relationship between portlandite and calcite. Note that the choice of mechanisms would have a direct impact on the kinetics of carbonation. A dissolution−precipitation mechanism would lead to carbonation rates orders of magnitude higher than those of a solid-state reaction,[25] especially at the relevant P/T conditions at which the above-mentioned carbonation processes typically take place (T < 100 °C).[26]

Another important aspect related to the better understanding of the mechanisms of portlandite carbonation refers to the formation (or otherwise) of a passivating product layer which will affect both the reaction kinetics and the $CaCO_3$ yield. The implications of the formation of such a passivating layer are manifold: while its formation would be detrimental during CCS, it would have a positive effect (delay) during cement degradation. Despite some efforts,[24] little is known regarding the formation of porosity/fractures or impervious product layers during portlandite carbonation.

The main aim of this study is to gain insights into the mechanisms of portlandite dissolution and carbonation as well as to investigate the crystallographic control in the advancement of the process. With these purposes in mind, in situ observations during dissolution and carbonation of cleaved and growth surfaces of portlandite single crystals were performed using an O-ring sealed fluid cell coupled to an Atomic Force Microscope (AFM). To our knowledge, this is the first study that succeeds in exploring the reactivity (dissolution and carbonation) of portlandite in situ at the nanoscale. These observations were complemented with ex situ carbonation experiments and the subsequent analysis of partially carbonated portlandite crystals using Field Emission Scanning Electron Microscopy (FESEM) and two-dimensional X-ray Diffraction (2D-XRD).

METHODOLOGY

Synthesis of Portlandite Crystals. $Ca(OH)_2$ single crystals large enough to perform AFM and 2D-XRD analyses were prepared by a modified counter-diffusion method[27] by mixing 0.2 M NaOH and 0.1 M $CaCl_2$ solutions. 50 mL of each of these solutions was placed in separate beakers and subsequently placed in a 2 L container, completely filled with deionized water and covered with paraffin wax in order to avoid exchange of CO_2 between the solution and the atmosphere, thus preventing the early carbonation of the portlandite crystals. A schematic representation of the setup in which crystallization of portlandite single crystals was performed is shown in Figure S1 (Supporting Information). The crystals obtained were clear, millimeter-sized hexagonal prisms (axis of the prism--c). Nontwinned, well shaped crystals were selected for the AFM experiments and kept growing in the container until their size reached about 4 mm length and 2 mm width. Crystals were collected, rinsed thoroughly in ethanol, and oven-dried for 30 min at 100 °C. Purity and phase analysis of the synthetic portlandite crystals were confirmed by XRD (Philips PW-1710 diffractometer with Cu Kα radiation, λ = 1.5406 Å). The morphology of portlandite single crystals was analyzed with the aid of a LEO Carl Zeiss GEMINI-1530 FESEM after coating the samples with carbon.

Ex Situ Carbonation of Portlandite Single Crystals. Portlandite crystals were placed in an air-ventilated plastic container at fixed RH (~93%) and temperature (20 ± 2 °C). Crystals were taken from the container at different time periods, weighed, carbon-coated, and then examined under the

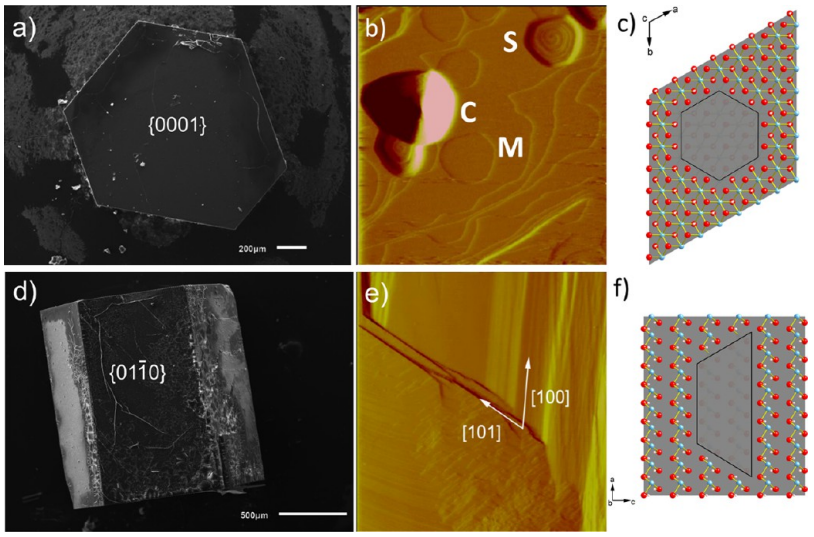

Figure 1. a) FESEM secondary electron image of a crystal obtained by the counter-diffusion method. The {0001} portlandite growth form surface is parallel to the image plane. b) AFM deflection image of the {0001} portlandite surface during dissolution in deionized water. Three types of etch pits are observed: monolayer-deep etch pits (M), concentric (C), and spiral hexagonal pits (S). Image size 5 × 5 μm. c) The structure of portlandite projected along ⟨001⟩. The morphology and crystallographic orientation of the edges of etch pits observed in (b) is outlined. Atoms: calcium: blue; oxygen: red; hydrogen: white. d) FESEM secondary electron image of a crystal obtained by the counter-diffusion method. The {01$\bar{1}$0} portlandite growth form surface is parallel to the image plane. e) AFM deflection image of the (01$\bar{1}$0) portlandite surface during dissolution in deionized water. Image size 5 × 5 μm; f) the structure of portlandite projected along ⟨110⟩. The morphology and crystallographic orientation of the edges of etch pits observed in (e) is outlined. Atoms: calcium: blue; oxygen: red; hydrogen: white.

FESEM. After one year of reaction, crystals were embedded in epoxy resin and cut parallel to the basal and prismatic planes for FESEM observation. To determine parent/product crystallographic orientation relationship(s), partially reacted crystals were collected at different time intervals during 4 months of carbonation time and analyzed using an X-ray single crystal diffractometer equipped with an area detector (D8 SMART APEX, Bruker). Pole figures describing the 3D orientation relationships between portlandite pseudomorphs and calcite were determined in this way. For these 2D-XRD experiments, the working conditions were as follows: Mo Kα (λ = 0.7093 Å), 50 kV, and 30 mA, a pinhole collimator of 0.5 mm in diameter, and an exposure time of 20 s per frame. Portlandite pseudomorphs were analyzed resting flat either on (0001) or on {01$\bar{1}$0} faces (diffractometer ω and 2θ angles were set at 10 and 20 degrees, respectively). A set of frames (2D diffraction patterns) was registered while rotating the sample round φ angle (a frame every 5 degrees; a total of 72 frames). Pole figures were calculated and displayed in stereographic projection using the XRD2DScan software.[28]

In Situ AFM Experiments. Freshly cleaved {0001} portlandite surfaces, ca. 2 × 2 × 1 mm in size, and {01$\bar{1}$0} growth surfaces, ca. 4 × 2 × 1 mm in size, were used as substrates for the experiments. In situ observations of these surfaces during dissolution in a drop of CO_2-free deionized water and carbonation in deionized water equilibrated with atmospheric CO_2 were performed using a fluid cell (Figure S2) of a Digital Instruments Nanoscope III Multimode AFM working in contact mode under ambient conditions (T = 23 °C). AFM images were collected using Si_3N_4 tips (Veeco Instruments, tip model NP-S20) with spring constants 0.12 N m^{-1} and 0.58 N m^{-1}. Images were analyzed using the NanoScope software (Version 5.31r1).

The evolution of the chemistry of the solution formed on the surface of portlandite crystals in contact with atmospheric CO_2 (ex situ carbonation experiments) as well as that of the solution in contact with crystals placed in a carbonate solution (in situ AFM experiments) was simulated using PHREEQC geochemical code.[29]

RESULTS AND DISCUSSION

Portlandite Morphology and Dissolution Features of {0001} and {01$\bar{1}$0} Surfaces. {0001} and {01$\bar{1}$0} are the main growth forms of portlandite crystals obtained by the counter-diffusion method (Figures 1a and 1d). These growth surfaces are typically flat and smooth in appearance, which could be indicative of a layer by layer growth mechanism, initiated either by screw-dislocations or by 2-dimensional nucleation.[30] The {01$\bar{1}$0} prismatic form is less relevant in mortars or cement, as in these cases portlandite crystals are mainly plate-like,[11,12] and thus this form represents a smaller proportion of the overall surface area of the crystal.

Figure S3 shows a typical sequence of AFM deflection images of the {0001} portlandite surface during dissolution in deionized water. The reaction proceeded by the formation and propagation of hexagonal etch pits. The observed steps had a height of ca. 0.3 nm, which corresponds to a $Ca(OH)_2$ monolayer. Three types of etch pits were observed: monolayer-deep etch pits randomly distributed on the flat surface (M, density ca. 0.8 × 10^8 cm^{-2}), concentric (C) (i.e., those of depth higher that one monolayer but not nucleated at screw dislocations) and spiral hexagonal pits (S) (Figure 1b). The latter two (density ca. 0.2 × 10^8 cm^{-2}) most likely originate at structural defects and screw dislocations, respectively. Single, isolated pits of one monolayer height nucleated either at defect-free surfaces or point defects.[30] Etch pit spreading rates were measured in spiral hexagonal pits as they allowed the determination of the individual spreading rate for each of the sides of the pit (Figure S4a). Initially, the (average) spreading rate was approximately constant (0.96 ± 0.05 nm s^{-1}), and it decreased significantly when the solution was approaching equilibrium (i.e., saturation with respect to portlandite) (Figure

S4b). In contrast, {01$\bar{1}$0} growth surfaces dissolved by retreatment of pre-existing steps as well as by the formation and spreading of deep, trapezium-like etch pits that rapidly elongated parallel to ⟨100⟩ (Figure 1e). It was not possible to quantify the dissolution kinetics of {01$\bar{1}$0} growth surfaces from measurements of sequential AFM images due to the very fast spreading of etch pits formed in those faces (dissolution was much faster than for the case of the {0001} form).

In order to understand the growth form of portlandite crystals and the nanoscale features of their dissolution, it is necessary to consider the particularities of its structure. $Ca(OH)_2$ is a layer compound; the layers are built with distorted edge-sharing CaO_6 octahedra. Each hydroxyl group is linked to three Ca atoms in its layer and surrounded by three other hydroxyl groups belonging to the adjacent layer (Figure 1c). The O−H vector is perpendicular to the (0001) plane, and the H atom forms hydrogen bonds to three oxygen atoms on the adjacent portlandite sheet. The {0001} growth slice, of thickness 3.03 Å, has a flat character[31] and contains three nonparallel but symmetrically equivalent ⟨100⟩ periodic bond chains (PBCs, uninterrupted chains of strong bonds between units building the crystal). The three PBCs in this face are chains of edge-sharing CaO_6 octahedra parallel to the equivalent [100], [010], and [110] directions. These are strong PBCs, linked by Ca−O bonds (Figure 1c). The {01$\bar{1}$0} growth slice has also a flat character and contains three nonparallel PBCs along ⟨100⟩, ⟨101⟩, and ⟨001⟩ (Figure 1f). ⟨101⟩, ⟨10$\bar{1}$⟩, and ⟨001⟩ PBCs present in the (01$\bar{1}$0) face are formed by chains of CaO_6 octahedra linked by hydrogen bonds. Flat faces commonly grow by a layer-spreading mechanism. The growth velocity of stepped and kink faces (those which contain one and none PBCs, respectively) is normally faster than that of flat faces. Usually, stepped and kinked faces are absent from the equilibrium crystal morphology, which is bounded by faces with flat character. This is fully in agreement with our observations showing that {0001} and {01$\bar{1}$0} were the dominant growth surfaces observed in the synthetically grown portlandite crystals and that these growth forms are apparently flat and smooth. PBCs contained in a crystal face represent the most probable directions of straight step edges occurring on such a face during dissolution. The angular relationships between step edges of etch pits observed in the AFM dissolution experiments of cleaved basal planes confirm that they are parallel to [100], [010], and [110] directions. As discussed above, these directions correspond to the three symmetrically equivalent ⟨100⟩ PBC directions. In the case of {01$\bar{1}$0}, the observed etch pit morphology agrees with the PBC hierarchy and structure of these portlandite surfaces (Figure 1f).

Pathways of Portlandite Carbonation Reaction. In situ AFM carbonation experiments of portlandite {0001} cleavage surfaces upon contact with carbonate-bearing aqueous solutions revealed that the reaction occurred by the fast dissolution of the portlandite substrate and the subsequent (nearly instantaneous) oriented precipitation of thick nuclei or three-dimensional islands. The etch pit density is significantly increased in the presence of carbonate ions (etch pit density ca. 5×10^9 cm^{-2}, see Figure S5), in agreement with the increase in dissolution rates of similar hydroxides ($Mg(OH)_2$) observed with increasing carbonate concentration.[2] This effect could be due to the adsorption (physisorption) of these ions onto defect-free calcite surfaces and subsequent competition for hydration water between this ion and the water adsorbed onto the calcite surface. Three dimensional islands tended to grow perpendicular to the surface, reaching heights of up to 235 nm immediately after the injection of the CO_2-bearing solution (Figures 2a to 2c). The observed nucleation density was ca. 7.4

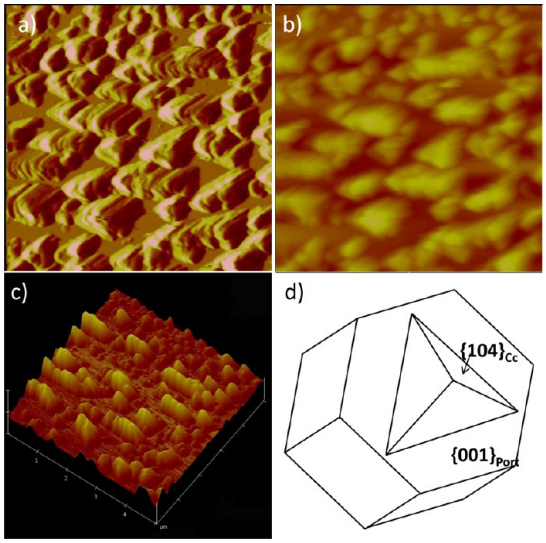

Figure 2. Deflection (a), height (b), and 3D deflection (c) AFM images of the {0001} portlandite surface after contact with carbonate-bearing solution. d) SHAPE simulation of the epitaxial relationship between portlandite and calcite: $\langle 001\rangle_{Port} \parallel \langle 001\rangle_{Cc}$.

$\times 10^8$ cm^{-2}, a value which is slightly lower than the etch pit density observed in dissolution experiments in the presence of carbonate ions. This suggests that for a calcite island to nucleate on the portlandite surface at least an etch pit has to form before in order to supply calcium ions for carbonate precipitation. During the time scale of the AFM experiments (total time ca. 60 min), the coalescence of these islands was not detected. Islands showed well-defined edges, which can be considered as an indication of the crystalline character of the newly formed phase, and were clearly oriented on the portlandite surface (Figures 2a to 2c). Modeling of calcite growth onto the {0001} portlandite surface using SHAPE software (http://www.shapesoftware.com/) shows a good agreement with the morphology of the carbonate island observed using AFM (Figure 2d). Figure S6 shows a full sequence of AFM images collected during the growth of these islands. These results suggest that portlandite carbonation in a water-rich environment occurs via a coupled dissolution−precipitation reaction.[25]

FESEM observations of portlandite crystals, that had been partially carbonated in a high relative humidity atmosphere, showed that carbonation in air resulted (as in the case of carbonation from aqueous solutions) in pseudomorphs that fully preserved the external hexagonal, prismatic shape of the original portlandite crystals, bounded by {0110} and {0001} forms (Figure 3a and 3b). Indeed, a closer look at the surface of such partially reacted portlandite crystals revealed the presence of protuberances or 3D-islands on both basal and prismatic faces (insets in Figure 3a and 3b). Interestingly, dissolution and corrosion features were still visible (despite the precipitate covering the surface) in both basal and, above all, prismatic faces. These observations support the idea that a similar mechanism operates during both carbonation of portlandite crystals in aqueous solution (AFM results) and in air at high relative humidity (FESEM observations).

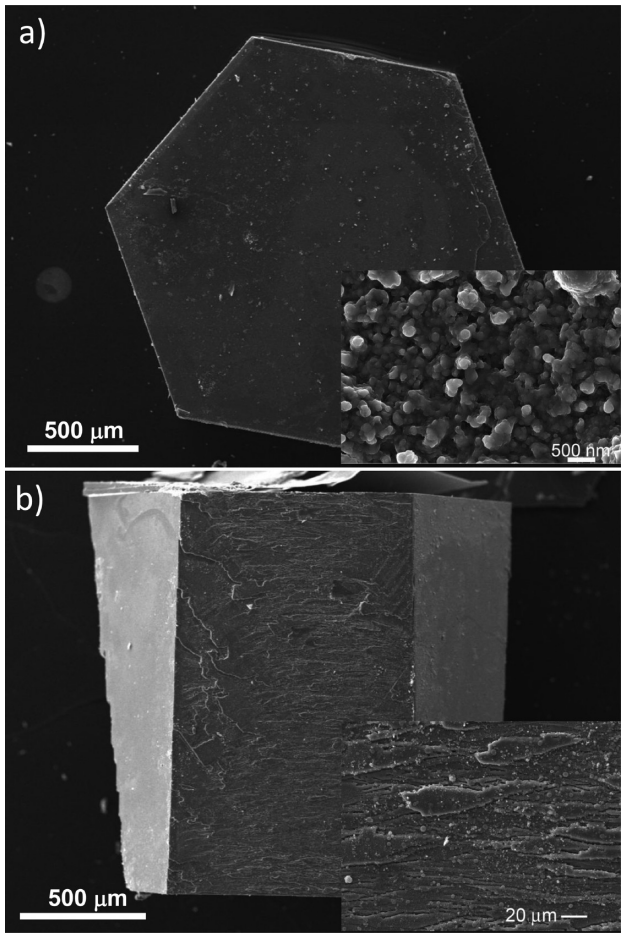

Figure 3. FESEM secondary electron images of a portlandite pseudomorph after 2 weeks contact with atmospheric CO_2 (T = 20 °C, RH = 93%). (a) Basal surface. The inset shows a detail of the protuberances or nuclei present at the surface. (b) Lateral view of the pseudomorph. The inset shows a detail of the prismatic surfaces of the partially replaced crystal where cracks are clearly visible.

However, the mechanism of portlandite carbonation reaction in air is still a matter of controversy. When water is virtually absent from the reaction medium, this reaction can be considered as the typical solid−gas reaction, which is kinetically favored at high T ($T \gg 100$ °C).[25] Nevertheless, under the conditions of our ex situ carbonation experiments (T = 20 °C and RH = 93%), there are 7 monolayers of water molecules adsorbed on portlandite surfaces.[21] It has been suggested that, above a certain critical amount of adsorbed water (four monolayers, corresponding to 75% RH at STP), the presence of this adsorbed water has a "catalytic effect" on portlandite carbonation.[21] Conversely, carbonation rates are virtually zero at room T when $pH_2O \rightarrow 0$.[11,25] The adsorbed multilayer film behaves as a liquid-like nanometric phase. Thus, carbonation in air under high RH conditions could also occur via a coupled dissolution−precipitation reaction. It should be mentioned that once the carbonation reaction is triggered, additional water is produced as a byproduct of carbonation via the (overall) reaction $Ca(OH)_2 + CO_2 \leftrightarrow CaCO_3 + H_2O$. Portlandite can dissolve in the adsorbed water layers, thus leading to the release of Ca^{2+} and OH^- ions to this interfacial fluid, thereby increasing the pH (up to 12.4).[10] CO_2 from the atmosphere also dissolves into this alkaline solution and subsequently hydrolyzes to give bicarbonate and carbonate ions, according to the equilibrium

$$\begin{aligned} CO_2(g) &\leftrightarrow CO_2(aq) + H_2O \\ &\leftrightarrow H_2CO_3 \\ &\leftrightarrow HCO_3^- + H^+ \\ &\leftrightarrow CO_3^{2-} + 2H^+ \end{aligned}$$

As a result, supersaturation is reached with respect to calcite within the interfacial or boundary water layer, and 3D islands, as seen in AFM experiments, can nucleate and grow onto portlandite surfaces.

In the case of both carbonation in solution and in air, at a high RH atmosphere, the presence of water would not have a purely catalytic effect but it would rather influence or control the reaction mechanism itself which involves a dissolution/precipitation reaction. Further evidence supporting this mechanism arises from the crystallographic relationships between portlandite and calcite (see below).

This mechanistic interpretation is in agreement with observations by numerous researchers that found that nonzero water activity is required for carbonation to proceed.[12,21,24,32] Note that the presence of water is not required during solid-state carbonation. In contrast, water is critical during interface-coupled dissolution−precipitation reactions.

Volume Change and Porosity Development during Portlandite Carbonation. One of the issues regarding the pseudomorphic replacement of portlandite by calcite is the higher molar volume of the product phase (calcite) as compared to the parent phase (portlandite), which may result in the arrest of the replacement progress.[24] However, differences in solubility between parent and product phases (i.e., the parent phase being more soluble than the product phase, as in the case of portlandite $-K_{sp} = 5.02 \times 10^{-6}$ - and calcite $-K_{sp} = 3.36 \times 10^{-9}$) may facilitate the generation of porosity and the progress of the coupled dissolution−precipitation reaction front in systems where the molar volume of the product phase is higher than that of the parent phase (i.e., the system studied here).[25] These differences in solubility are taken into account in PHREEQC simulations. According to these simulations, if a portlandite crystal dissolves in a 12.1 Å layer of water (i.e., the thickness of the 7 water monolayers adsorbed onto portlandite surfaces at RH = 93%) in equilibrium with air (i.e., $pCO_2 = 10^{-3.398}$), the resulting solution will reach saturation with respect to calcite when 5.89×10^{-14} moles of portlandite per cm^2 are dissolved, which represents an amount significantly smaller than that corresponding to a complete portlandite monolayer (2.77×10^{-10} moles). However, the previous value matches that corresponding to the dissolution of a $Ca(OH)_2$ monolayer if we consider the etch pit density observed during AFM dissolution experiments.

The ΔV of the reaction can be calculated using the equation[33]

$$\Delta V_{reaction} = 100 \cdot \left(\frac{n_d}{n_p} \cdot \frac{V_{M,Cc}}{V_{M,Port}} - 1 \right)$$

where n_d is the amount of moles of portlandite dissolved, n_p is the amount of moles of calcite precipitated, $V_{M,Port}$ is the molar volume of portlandite (32.81 cm^3/mol), and $V_{M,Cc}$ is the molar volume of calcite (36.90 cm^3/mol). Both n_d and n_p are calculated using PHREEQC. If a complete portlandite monolayer dissolves into such a layer of adsorbed water in

equilibrium with air and, subsequently, calcite precipitates, $\Delta V_{reaction}$ would be positive (12.5%). Thus, porosity is not expected to be generated during this replacement reaction. This would be the case if calcite precipitates as a continuous surface layer over the whole portlandite surface. However, this is not what we observed during AFM experiments: discrete calcite island (a few hundred nm high) formed instead. For complete passivation to occur (i.e., zero porosity of the surface precipitate), the thick 3D islands should merge as they grow, but the amount of portlandite dissolved at this point cannot be simply estimated considering differences in molar volumes or relative solubility of the two phases involved, and energetic considerations of the surfaces involved in the process must be taken into account. Full coverage of the portlandite surface is eventually reached, as shown by FESEM observations (Figure 4) and by the quantification of the evolution of the carbonation

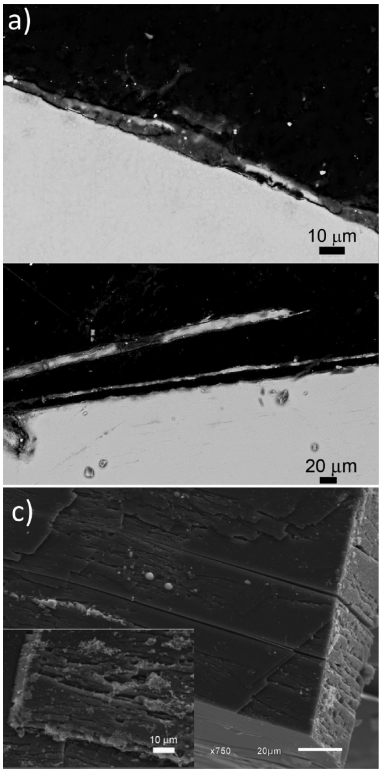

Figure 4. FESEM images of a portlandite pseudomorphs after 1 year contact with atmospheric CO_2 (T = 20 °C, RH = 93%). (a) Backscattered electron image of a thin replaced rim (darker upper layer) and the formation of cracks in the reaction product and the parent portlandite substrate. (b) Backscattered electron image of a section parallel to the prismatic faces of a partially replaced portlandite crystal embedded into a epoxy resin block. The detachment of layers parallel to the basal plane is observed. (c) Secondary electron image of the partially replaced portlandite crystal where cracks parallel to the basal plane are observed. The inset shows a detail of the lateral surface of the crystal.

reaction determined from the weight measurements of portlandite single crystals kept in air under high RH (~93%) for different periods of time. This latter analysis showed that the reaction occurred at a very slow rate after 20 days (i.e., ca. constant weight of the crystal is reached after this time). Within this period, the degree of transformation was ~1.5% (Figure S7). FESEM observations of cross sections of partially replaced crystals show that a product layer of a minimum thickness of ~3 μm forms (Figure 4a) before passivation of the surface occurs.

However, porosity is not the only pathway for the fluid to reach the surface of the unreacted solid. Our FESEM observations of partially replaced crystals showed the formation of a significant amount of cracks that in the prismatic faces were parallel to the basal plane and eventually led to the detachment of thin slices from the crystal (Figure 4b and 4c). The replacement of a mineral phase by another with higher molar volume was studied by Jamtveit and co-workers[34] for the case of leucite-analcime. Such a replacement results in accumulation of stress at the interface, which finally leads to fracturing. Our observations suggest that in fact fractures form in response to the stresses generated in the replacement rim due to the positive volume change during the transformation of portlandite into calcite. These fractures are critical in the progress of the reaction, as they expose fresh, unreacted portlandite surfaces to the reaction fluid that subsequently also shows evidence of carbonation. Therefore, they allow the advancement of the reaction front even in the cases where no porosity development is expected from the relative molar volume changes and solubility differences between parent and product phases, as in this case.

Crystallographic Control in the Replacement of Portlandite by Calcite. Our AFM observations show carbonate islands with a clear preferred crystallographic orientation on the portlandite substrate, thus indicating that their precipitation is somehow crystallographically controlled. 2D-XRD analyses confirmed that the product of the reaction was calcite. Furthermore, the (104) calcite pole figure indicated a strong preferred (epitactic) crystallographic orientation of calcite formed after carbonation of portlandite single crystals (Figure 5). Characteristic rings occur due to the lack of axis symmetry along calcite [001] axis.

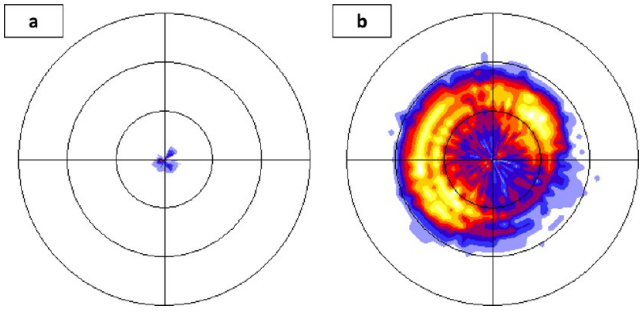

Figure 5. Pole figures (PF) obtained from 2DRXD analysis showing the crystallographic orientation relationship between the primary portlandite crystal and the overgrown calcite: $[001]_{Cc}$ // $[001]_{Cc}$. a) PF for (0001) portlandite and b) PF for (104) calcite after 4 months carbonation in air at 93% RH.

The analysis of the pole figure suggests the following orientation relationship: $\langle 001\rangle_{Cc}$ // $\langle 001\rangle_{Port}$, which implies that $\{0001\}_{Cc}$ ‖ $\{0001\}_{Port}$. As stated above, this orientation relationship was simulated using SHAPE software. The simulation showed a good agreement between the simulated morphology and the morphology of the calcite islands nucleated on portlandite cleavage surfaces observed in the AFM experiments (Figure 2). In a solid-state reaction, the OH^- groups in the basal planes would be replaced (dehydration) by CO_3^{-} ions (carbonation). Energetically, this could be a favorable process. However, such a direct replacement would

lead to a pseudomorph with a topotactic relationship between parent and product phases. This is not what our 2D-XRD results show, which suggests an epitactic relationship. It seems that, locally, the solution completely dissolves the $Ca(OH)_2$ structure, closely followed by the epitaxial formation of thick pseudopyramidal calcite islands on the remaining portlandite. The structural misfit (mf) between two directions in the $\{0001\}_{Port}$ and $\{0001\}_{Cc}$ planes can be calculated using the equation[35]

$$\text{mf}\,(\%) = \frac{2(t_{[uvw]Port} - t_{[uvw]Cc})}{t_{[uvw]Port} + t_{[uvw]Cc}}$$

where $t_{[uvw]}$ is the repeating period along the [uvw] direction in portlandite (Port) and calcite (Cc). The misfit determined for example along $[100]_{Port}$ and $[100]_{Cc}$ in (0001) portlandite and calcite planes is 33%. This high mismatch precludes the formation of continuous replacement calcite layers onto portlandite {0001} surfaces. Instead, thick three-dimensional islands form. However, along the *c*-axis the misfit determined is 14%, which is within the limits for epitaxial growth. The carbonate islands formed, although oriented with the *c* axis parallel to each other and to the *c* axis of the underlying portlandite single crystal, are slightly rotated along their *c* axis (Figure 2a). Apparently, such a rotation occurs in order to accommodate the stress and resulting strain developed at the interface as a consequence of the misfit between portlandite and calcite structures (Figure 6). This process precludes the early arresting of the carbonation process that could take place upon the formation of a continuous calcite surface layer a few nm thick. Instead, a thicker layer of product is formed until the empty spaces between single crystals are closed. In contrast, a solid-state topotactic replacement would have resulted in the formation of a nonporous product layer once a single portlandite monolayer transformed into calcite.

Implications. Our results show that carbonation of portlandite, both in aqueous solution and in a high relative ambient humidity, occurs via a tight interface-coupled dissolution–precipitation process.[25] The model proposed here for the carbonation of portlandite crystals explains all the observed features of the parent and product phases as well as the kinetics of such a replacement process. These results may have implications for technological issues such as the setting of traditional lime mortars, carbonation of Portland cement or concrete degradation as well as on the kinetics and yield during ex situ CCS by mineral carbonation of Ca-rich industrial wastes. In all the aforementioned cases demonstration that portlandite carbonation occurs as a consequence of an interface-coupled dissolution–precipitation reaction is critical for the correct implementation of such a process in the formulation of geochemical codes aimed at quantifying reaction rates. This provides a novel framework to accurately evaluate the long-term aqueous durability of concrete in dams or radioactive waste disposal facilities as well as in CO_2 injection wells or the kinetics of cement and lime mortar carbonation. Finally, because mineral carbonation could have a great potential in the fixation of atmospheric CO_2,[5,36] the knowledge gained in this study may help in the development of optimized strategies for the capture of CO_2 and its long-term storage in minerals.

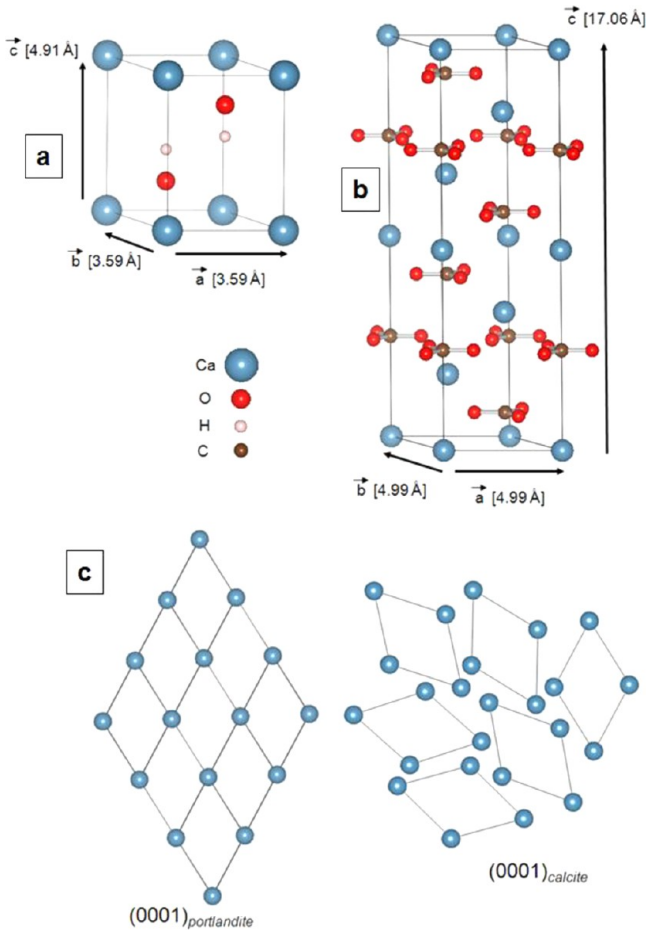

Figure 6. Portlandite (a) and calcite (b) unit cells. (c) Schematic representation of the epitaxial relationship found after the replacement of portlandite by calcite via interface-coupled dissolution–precipitation carbonation progressing parallel to the basal plane.

■ ASSOCIATED CONTENT

Supporting Information

Further information of portlandite single crystal synthesis, kinetics of dissolution and carbonation, and portlandite crystal structure as well as full sequences of images of AFM carbonation and dissolution experiments. This material is available free of charge via the Internet at http://pubs.acs.org.

■ AUTHOR INFORMATION

Corresponding Author

*Phone: +34958240473. Fax: +34958243368. E-mail: encaruiz@ugr.es.

Author Contributions

The manuscript was written through contributions of all authors. All authors have given approval to the final version of the manuscript. All authors contributed equally.

Notes

The authors declare no competing financial interest.

■ ACKNOWLEDGMENTS

This research project was funded by the European Commission (grant MRTN-CT-2006-035488), the Spanish government (grants MAT2012-37584 and CGL2012-35992), and the Junta de Andalucía (research group RNM-179 and project P11-RNM-7550). E. Ruiz-Agudo also acknowledges the receipt

of a Ramón y Cajal grant from Spanish Ministry of Economy and Competitivy. The research at the University of Münster is also supported by the Deutsche Forschungsgemeinschaft (DFG).

REFERENCES

(1) Zhao, L.; Sang, L.; Chen, J.; Ji, J.; Teng, H. H. Aqueous carbonation of natural brucite: relevance to CO_2 sequestration. *Environ. Sci. Technol.* **2010**, *44* (1), 406−411.
(2) Hövelmann, J.; Putnis, C. V.; Ruiz-Agudo, E.; Austrheim, H. Direct nanoscale observations of CO_2 sequestration during brucite [$Mg(OH)_2$] dissolution. *Environ. Sci. Technol.* **2012**, *46*, 5253−5260.
(3) Jordan, G.; Rammensee, W. Dissolution rates and activation energy for dissolution of brucite (001): A new method based on the microtopography of crystal surfaces. *Geochim. Cosmochim. Acta* **1996**, *60* (24), 5055−5062.
(4) Baranek, Ph.; Lichanot, A.; Orlando, R.; Dovesi, R. Structural and vibrational properties of solid $Mg(OH)_2$ and $Ca(OH)_2$ − performances of various hamiltonians. *Chem. Phys. Lett.* **2001**, *340* (3−4), 362−369.
(5) Lackner, K. S. Carbonate chemistry for sequestering fossil carbon. *Annu. Rev. Energy Environ.* **2002**, *27*, 193−232.
(6) Hashim, M. A.; Mukhopadhyay, S.; Sahu, J. N.; Sengupta, B. Remediation technologies for heavy metal contaminated groundwater. *J. Environ. Manage.* **2011**, *92*, 2355−23885.
(7) Kutchko, B. G.; Strazisar, B. R.; Szombak, D. A.; Lowry, G. V.; Thaulow, N. Degradation of well cement by CO_2 under geologic sequestration conditions. *Environ. Sci. Technol.* **2007**, *41*, 4787−4792.
(8) Sanna, A.; Dri, M.; Hall, M. R.; Maroto-Valer, M. Waste materials for carbon capture and storage by mineralisation (CCSM) - A UK perspective. *Appl. Energy* **2012**, *99*, 545−554.
(9) Kingery, W. D.; Vandiver, P. B.; Prickett, M. The beginnings of pyrotechnology, part II: production and use of lime and gypsum plaster in the pre-pottery Neolithic Near East. *J. Field Archaeol.* **1988**, *15*, 219−244.
(10) Cizer, Ö.; Rodriguez-Navarro, C.; Ruiz-Agudo, E.; Elsen, J.; Van Gemert, D.; Van Balen, K. Phase and morphology evolution of calcium carbonate precipitated during carbonation of hydrated lime pastes. *J. Mater. Sci.* **2012**, *47* (16), 6151−6165.
(11) Elert, K.; Rodriguez-Navarro, C.; Sebastian Pardo, E.; Hansen, E.; Cazalla, O. Lime mortars for the conservation of historic buildings. *Stud. Conserv.* **2002**, *47*, 62−75.
(12) Yang, T.; Keller, B.; Magyari, E.; Hametner, K.; Günther, D. Direct observation of the carbonation process on the surface of calcium hydroxide crystals in hardened cement paste using an Atomic Force Microscope. *J. Mater. Sci.* **2003**, *38* (9), 1909−1916.
(13) Ryu, J.-S.; Otsuki, N.; Minagawa, H. Long-term forecast of Ca leaching from mortar and associated degeneration. *Cem. Concr. Res.* **2002**, *32* (10), 1539−1544.
(14) Marinoni, N.; Pavese, A.; Voltolini, M.; Merlini, M. Long-term leaching test in concretes: An X-ray powder diffraction study. *Cem. Concr. Compos.* **2008**, *30* (8), 700−705.
(15) Uibi, M.; Uus, M.; Kuusik, R. CO_2 mineral sequestration in oil-shale wastes from Estonian power production. *J. Environ. Manage.* **2009**, *90*, 1253−1260.
(16) Huntzinger, D. N.; Gierke, J. S.; Kawatra, K.; Eisele, T. C.; Sutter, L. L. Carbon dioxide sequestration in cement kiln dust through mineral carbonation. *Environ. Sci. Technol.* **2009**, *43*, 1986−1992.
(17) Montez-Hernandez, G.; Pérez-López, R.; Renard, F.; Nieto, J. M.; Charlet, L. Mineral sequestration of CO_2 by aqueous carbonation of coal combustion fly-ash. *J. Hazardous Mater.* **2009**, *161*, 1347−1354.
(18) Huijgen, W. J. J.; Witkamp, G. J.; Comans, R. N. J. Mineral CO_2 sequestration by steel slag carbonation. *Environ. Sci. Technol.* **2005**, *39* (24), 9676−9682.
(19) Moorehead, D. R. Cementation by the carbonation of hydrated lime. *Cem. Concr. Res.* **1986**, *16*, 700−708.
(20) Johnstone, J. R.; Glasser, F. P. Carbonation of portlandite single crystals and portlandite in cement paste. *9th International Congress on the Chemistry of Cement* **1992**, *5*, 370−376.
(21) Beruto, D. T.; Botter, R. Liquid-like H_2O adsorption layers to catalyze the $Ca(OH)_2/CO_2$ solid−gas reaction and to form a non-protective solid product layer at 20 °C. *J. Eur. Ceram. Soc.* **2000**, *20*, 497−503.
(22) Gillott, J. E. Carbonatation of $Ca(OH)_2$ investigated by thermal and X-ray diffraction methods of analysis. *J. Appl. Chem.* **1967**, *17*, 185−189.
(23) Stepkowska, E. T. Hypothetical transformation of $Ca(OH)_2$ into $CaCO_3$ in solid-state reactions of portland cement. *J. Therm. Anal. Calorim.* **2005**, *80* (3), 727−733.
(24) Montes-Hernandez, G.; Daval, D.; Chiriac, R.; Renard, F. Growth of nanosized calcite through gas−solid carbonation of nanosized portlandite under anisobaric conditions. *Cryst. Growth Des.* **2010**, *10* (11), 4823−4830.
(25) Putnis, A. Mineral Replacement Reactions. In *Thermodynamics and Kinetics of Water-Rock Interaction*; Oelkers, E. H., Schott, J., Eds.; *Rev. Mineral. Geochem.* **2009**, *30*, 87−124.
(26) Beruto, D. T.; Barberis, F.; Botter, R. Calcium carbonate binding mechanisms in the setting of calcium and calcium−magnesium putty-limes. *J. Cult. Herit.* **2005**, *6*, 253−260.
(27) Johnston, J. The utilization of diffusion processes in the preparation of pure substances. *J. Am. Chem. Soc.* **1914**, *36*, 16−19.
(28) Rodriguez-Navarro, A. B. XRD2DScan: new software for polycrystalline materials characterization using two-dimensional X-ray diffraction. *J. Appl. Crystallogr.* **2006**, *39*, 905−909.
(29) Parkhurst, D. L.; Appelo, C. A. J. Users guide to PHREEQC (version 2) − a computer program for speciation, batch reaction, one dimensional transport, and inverse geochemical calculations. *U.S. Geological Survey Water-Resources Investigation Report 99-4259*; 1999; 312pp.
(30) Ruiz-Agudo, E.; Putnis, C. V. Direct observations of mineral-fluid reactions using atomic force microscopy: the specific example of calcite. *Mineral. Mag.* **2012**, *76*, 227−253.
(31) Hartman, P.; Perdok, W. G. On the relations between structure and morphology of crystals. I. *Acta Crystallogr.* **1955**, *8*, 49−52.
(32) Shih, S. M.; Ho, C. S.; Song, Y. S.; Lin, J. P. Kinetics of the reaction of $Ca(OH)_2$ with CO_2 at low temperature. *Ind. Eng. Chem. Res.* **1999**, *38* (4), 1316−1322.
(33) Pollok, K.; Putnis, C. V.; Putnis, A. Mineral replacement reactions in solid solution-aqueous solution systems: Volume changes, reactions paths and end-points using the example of model salt systems. *Am. J. Sci.* **2011**, *311* (3), 211−236.
(34) Jamtveit, B.; Putnis, C. V.; Malthe-Sorenssen, A. Reaction induced fracturing during replacement processes. *Contrib. Mineral. Petrol.* **2009**, *157*, 127−133.
(35) Bonev, I. On the terminology of the phenomena of mutual crystal orientation. *Acta Crystallogr.* **1972**, *A28*, 508−512.
(36) Regnault, O.; Lagneau, V.; Schneider, H. Experimental measurement of portlandite carbonation kinetics with supercritical CO_2. *Chem. Geol.* **2009**, *265* (1−2), 113−121.